Solution ^{1}H NMR Investigation of the Molecular and Electronic Structure of the Active Site of Substrate-Bound Human Heme Oxygenase: the Nature of the Distal Hydrogen Bond Donor to Bound Ligands

Carol M. Gorst,[†] Angela Wilks,[‡] Deok Cheon Yeh,[†] Paul R. Ortiz de Montellano,[‡] and Gerd N. La Mar*,[†]

Contribution from the Department of Chemistry, University of California, Davis, California 95616, and Department of Pharmaceutical Chemistry, University of California, San Francisco, California 94143

Received May 4, 1998

Abstract: The 265-residue soluble and completely active portion of inducible recombinant human heme oxygenase-1 (hHO), the enzyme responsible for heme catabolism, has been investigated by ^{1}H NMR to elucidate the molecular and electronic structure of the substrate-bound complex. 2D NMR of substrate-free hHO reveals a cluster of nine mobile aromatic residues whose signals are largely "bleached" upon binding high-spin hemin but reappear as new signals in the low-spin, cyanide-inhibited hHO-hemin complex. Unambiguous assignment of the heme and axial His25 signals in the latter complex allows placement of the aromatic clusters, as well as other TOCSY-detected side chains, into proximal, distal, or peripheral positions over specific pyrroles based on dipolar contacts and/or relaxation effects. The three aromatic clusters are located one on the proximal side adjacent to the axial His and the other two peripheral and distal to the pyrrole I/II junction, the site of heme oxidation. The density of heme methyl dipolar contacts, when compared to those of globins or peroxidases, reflects an "open" pocket, where hemin binds in the preformed aromatic cluster of hHO with pyrrole rings I and II and parts of pyrrole ring IV buried in the protein, with pyrrole ring III largely exposed to the solvent, and with the proximal side oriented toward the protein surface and the distal site toward the protein interior. A distal labile proton has been located which serves as the H-bond donor to cyanide, is the likely origin of the spectroscopically detected pK of ∼7.6 in the hHO-hemin complex, and probably arises from the same distal residue that serves as the H-bond donor to the activated O_2. Based on previous reports of inconsequential effects on HO activity upon mutating the conserved, non-heme-ligated His, the NMR detection of the conserved distal base in H132A-hHO-CN, together with the available NMR spectral parameters, we identify the distal base as a Tyr. The highly conserved His132 is found as one of two His groups involved in a strong, pseudosymmetric hydrogen-bonding network that dynamically stabilizes the active-site structure.

Introduction

Heme oxygenase (HO)[1] is a membrane-bound enzyme that catalyzes the regiospecific conversion[2] of heme to biliverdin IXα and CO. The enzyme exists in two isoforms with essentially identical activity, the inducible HO-1 being primarily involved in heme catabolism[3] and the constitutive HO-2 primarily serving as a source of CO,[4,5] a putative neural messenger.[6] Both enzymes have been cloned,[7−10] a truncated and completely active soluble, HO-1, has been expressed, and numerous mutants have been prepared.[11−14] The currently accepted intermediates in the stereoselective cleavage of the heme α-meso position are α-hydroxyheme, verdoheme, and Fe(III) biliverdin.[15,16] However, the mechanism of activation of the O_2 involved in the cleavage reaction and the basis of the

* Address correspondence to Gerd N. La Mar, Department of Chemistry, University of California, Davis, One Shields Avenue, Davis, CA 95616. Phone: (530) 752-0958. E-mail: lamar@indigo.ucdavis.edu.

† Department of Chemistry.

‡ Department of Pharmaceutical Chemistry.

(1) Abbreviations used: hHO, human heme oxygenase-1; rHO, rat heme oxygenase-1; HO-1, heme oxygenase isoform 1; TOCSY, 2D total correlation spectroscopy; NOESY, 2D nuclear Overhauser spectroscopy; Mb, myoglobin; PH, protohemin IX; WEFT, water-eliminated Fourier transform.

(2) Tenhunen, R.; Marver, H. S.; Schmid, R. *J. Biol. Chem.* **1969**, *244*, 6388−6394. Schacter, B. A.; Nelson, E. B.; Marver, H. S.; Masters, B. S. S. *J. Biol. Chem.* **1972**, *247*, 3601−3607.

(3) Yoshida, T.; Kikuchi, G. *J. Biol. Chem.* **1978**, *253*, 4224−4229. Yoshida, T.; Kikuchi, G. *J. Biol. Chem.* **1979**, *254*, 4487−4491.

(4) Maines, M. D.; Trakshel, G. M.; Kutty, R. K. *J. Biol. Chem.* **1986**, *261*, 411−419.

(5) Maines, M. D. *FASEB J.* **1988**, *2*, 2557−2568.

(6) Verma, A.; Hirsch, D. J.; Glatt, C. E.; Ronnett, G. V.; Snyder, S. H. *Science* **1993**, *259*, 381−384.

(7) Wilks, A.; Ortiz de Montellano, P. R. *J. Biol. Chem.* **1993**, *268*, 22357−22362.

(8) Wilks, A.; Black, S. M.; Miller, W. L.; Ortiz de Montellano, P. R. *Biochemistry* **1995**, *34*, 4421−4427.

(9) Ishikawa, K.; Sato, M.; Ito, M.; Yoshida, T. *Biochem. Biophys. Res. Commun.* **1992**, *182*, 981−986.

(10) Ishikawa, K.; Matera, K. M.; Zhou, H.; Fuji, H.; Sato, M.; Yoshimura, T.; Ikeda-Saito, M.; Yoshida, T. *J. Biol. Chem.* **1998**, *273*, 4317−4722.

(11) Sun, J.; Loehr, T. M.; Wilks, A.; Ortiz de Montellano, P. R. *Biochemistry* **1994**, *33*, 13734−13740.

(12) Wilks, A.; Sun, J.; Loehr, T. M.; Ortiz de Montellano, P. R. *J. Am. Chem. Soc.* **1995**, *117*, 2925−2926. Wilks, A.; Sun, J.; Loehr, T. M.; Ortiz de Montellano, P. R. *Biochemistry* **1996**, *35*, 930−936.

(13) Ito-Maki, M.; Ishikawa, K.; Mansfield Matera, K.; Sato, M.; Ikeda-Saito, M.; Yoshida, T. *Arch. Biochem. Biophys.* **1993**, *317*, 253−258.

(14) Wilks, A.; Ortiz de Montellano, P. R.; Sun, J.; Loehr, T. M. *Biochemistry* **1996**, *35*, 930−936.

(15) Beale, S. I. *Chem. Rev.* **1993**, *93*, 785−802.

S0002-7863(98)01547-9 CCC: $15.00
Published on Web 08/15/1998

stereoselectivity are still incompletely understood. In the absence of a crystal structure or sequence homology to other enzymes, a limited understanding of the active site of HO has been achieved on the basis of functional studies[17] using enzyme mutants[11,14,18] and modified hemes,[19,20] ligation rate comparison to globins,[21] and a variety of spectroscopic data.[3,11,22−27]

The mechanism by which HO exerts its remarkable stereoselectivity in attacking only the α-meso bridge is only partially understood, but both electronic and steric influences have been proposed. The stereoselectivity is enhanced by electron-donating and abolished by strongly electron-withdrawing α-meso substituents.[19,20] The pattern of unpaired spin density in rat HO-heme-CN also places the largest spin density on the α-meso position.[24] Both the ^{1}H NMR spectra[24] of HO-hemin-CN and resonance Raman spectra[27] of HO-heme-O_2 indicate that the axial ligands are strongly tilted from the heme normal. The strong steric effects suggested by these latter findings are consistent with the demonstration that HO-heme discriminates against CO relative to O_2 much more strongly than do the globins.[21]

The mechanism of O_2 activation, in contrast to that in cytochromes P450,[28] does not pass through a ferryl heme.[7] The strong similarities of the optical[3] and resonance Raman spectra[11,22,23] of the heme-CO complex to those of the same Mb complex argue for a neutral His as the axial ligand. The loss of activity caused by mutation of His25 to Ala that is rescued by the addition of imidazole establishes that His25 is the axial iron ligand.[8,22] Spectroscopic results on the oxidized HO-hemin complex have been interpreted[22,23] in terms of a ligated water linked strongly to a titratable distal base with pK ∼7.6. The similarity of the EPR, optical, and resonance Raman spectra, as well as the pK of the base, to those of the analogous Mb complexes have led to the expectation[23] that the distal base is a His. There are four universally conserved His groups in HO: His25, the axial ligand, and His84, 119, and 132. The latter has been favored as the distal base because it falls in a highly conserved segment thought to constitute the distal pocket. However, substitution[9,13,18] of each of the three remaining conserved His groups has excluded a His origin for the distal base.[29] Because of the strong hyperfine fields induced by the paramagnetic iron,[30−33] ^{1}H NMR of low-spin ferriheme enzymes is capable of directly detecting the labile protons that are hydrogen-bonded to bound ligands. In favorable cases, the nature of the residue side chain that provides this labile proton can be identified.

Preliminary ^{1}H NMR studies have been reported[24] for the recombinant rat HO-1 (rHO) hemin cyanide complex. In accord with other spectroscopic methods, the ^{1}H NMR data were consistent with a heme environment very similar to that of Mb in both the high-spin aquo and low-spin cyano complexes. It was also observed that the initial rHO-hemin complex bound the heme in a disordered manner about the α,γ-meso axis and that the equilibrium distribution of the two forms was ∼55:45. This nearly equal distribution of the two forms led to poor resolution and sensitivity and precluded the determination of structural details beyond demonstration of the heme rotational disorder and the observation of an unusual heme contact shift pattern based on partial heme assignments. Since these early ^{1}H NMR assignments on rHO, it has become obvious that human HO-1 (hHO) is superior to rHO for ^{1}H NMR studies because a much stronger preference (∼3:1) for one of the two heme orientations in hHO affords the higher sensitivity and resolution necessary for more definitive NMR studies.

We report herein a 2D ^{1}H NMR investigation of hHO, its hemin-bound complex, hHO-hemin, and the cyanide-inhibited substrate complex, hHO-hemin-CN. The study was designed to (a) more fully characterize the electronic structure of the heme, (b) assess the nature of the substrate-binding pocket before and after substrate binding, and (c) elucidate the nature of labile proton(s) for the distal base proposed to play a key role in activating bound O_2. In particular, since a His as the distal base is largely eliminated by mutagenesis[18] and by the present study of the H132A mutant, direct determination of the nature of the distal side chain should provide guidance for mutagenesis studies intended to establish the identity and exact role of the distal residue in the activation of O_2 and the stereoselectivity of heme cleavage.

Materials and Methods

Protein. Human heme oxygenase and the H132A mutant[29] were expressed and purified as previously described.[7] Elution of the heme-His132-hHO-1 complex from the BioGel HTP column yielded two peaks, the first having a Soret maximum at 400 nm and the second at 404 nm. The 404-nm fraction was used in all subsequent NMR studies.[29] Samples were prepared for NMR experiments by exchanging the solvent into either a 90% ^1H_2O, 10% ^2H_2O, or 98% ^2H_2O solution of 100 mM sodium phosphate using an Amicon filtration device. Samples of hHO-hemin failed to maintain a constant pH below pH ∼7.5, and slowly precipitated over the time necessary to collect useful

(16) Maines, M. D. *Heme-Oxygenase-Clinical Applications and Functions*; CRC Press: Boca Raton, FL, 1992.
(17) Ortiz de Montellano, P. R. *Acc. Chem. Res*. In press.
(18) Mansfield Matera, K.; Zhou, H.; Migita, C. T.; Hobert, S. E.; Ishikawa, K.; Katakura, K.; Maeshima, H.; Yoshida, T.; Ikeda-Saito, M. *Biochemistry* **1997**, *36*, 4909−4915.
(19) Torpey, J.; Ortiz de Montellano, P. R. *J. Biol. Chem.* **1996**, *271*, 26067−26073.
(20) Torpey, J.; Ortiz de Montellano, P. R. *J. Biol. Chem.* **1997**, *272*, 22008−22014.
(21) Migita, C. T.; Mansfield Matera, K.; Ikeda-Saito, M.; Olson, J. S.; Fujii, H.; Yoshimura, T.; Zhou, H.; Yoshida, T. *J. Biol. Chem.* **1998**, *273*, 945−949.
(22) Sun, J.; Wilks, A.; Ortiz de Montellano, P. R.; Loehr, T. M. *Biochemistry* **1993**, *32*, 14151−14157.
(23) Takahashi, S.; Wang, J.; Rousseau, D. L.; Ishikawa, K.; Yoshida, T.; Host, J. R.; Ikeda-Saito, M. *J. Biol. Chem*. **1994**, *269*, 1010−1014. Takahashi, S.; Wang, J. L.; Rousseau, D. L.; Ishikawa, K.; Yoshida, T.; Takeuchi, N.; Ikeda-Saito, M. *Biochemistry* **1994**, *33*, 5531−5538.
(24) Hernández, G.; Wilks, A.; Paolesse, R.; Smith, K. M.; Ortiz de Montallano, P. R.; La Mar, G. N. *Biochemistry* **1994**, *33*, 6631−6641.
(25) Hawkins, B. K.; Wilks, A.; Powers, L. S.; Ortiz de Montallano, P. R.; Dawson, J. H. *Biochim. Biophys. Acta* **1996**, *1295*, 165−173.
(26) Takahashi, S.; Matera, K. M.; Fujii, H.; Zhou, H.; Ishikawa, K.; Yoshida, T.; Ikeda-Saito, M.; Rousseau, D. *Biochemistry* **1997**, *36*, 1402−1410.
(27) Takahashi, S.; Ishikawa, K.; Takeuchi, N.; Ikeda-Saito, M.; Yoshida, T.; Rousseau, D. L. J. *Am. Chem. Soc.* **1995**, *117*, 6002−6006.
(28) Ortiz de Montellano, P. R. In *Cytochrome P450: Structure, Mechanism, and Biochemistry*, 2nd ed.; Ortiz de Montellano, P. R., Ed.; Plenum Press: New York, 1995; pp 245−304.
(29) A H132A mutation has been reported to both alter[14] and not alter[18] the spectroscopic and catalytic properties of HO-1. Altered HO-1 properties were observed[14] with the soluble recombinant human enzyme expressed in DH5α cells. However, recent work has shown that the soluble recombinant human protein expressed in BL21 cells closely resembles the wild-type enzyme. This finding is consistent with the report[18] that the recombinant rat enzyme obtained by refolding of protein expressed as inclusion bodies is also very similar to the wild-type. Although the reproducible misfolding or other alteration observed with the enzyme expressed in DH5α cells remains unclear, the results with the protein expressed in BL21 cells confirms that the human H132A mutant, like the corresponding rat enzyme,[18] exhibits spectroscopic and catalytic properties similar to those of the wild-type enzyme. His132 thus appears not to be a critical catalytic residue.
(30) Satterlee, J. D. *Annu. Rep. NMR Spectrosc.* **1986**, *17*, 79−178.
(31) Bertini, I.; Turano, P.; Vila, A. J. *Chem. Rev.* **1993**, *93*, 2833−2932.
(32) La Mar, G. N.; de Ropp, J. S. *Biol. Magn. Reson*. **1993**, *12*, 1−78.
(33) Lecomte, J. T. J.; Smit, J. D. G.; Winterhalter, K. H.; La Mar, G. N. *J. Mol. Biol*. **1989**, *209*, 235−247.

2D NMR data. For WT hHO-protohemin-CN (hHO-PH-CN), the majority of the data were collected on a sample ~2 mM in protein at pH 8.0, for which labile proton exchange was sufficiently slow to allow characterization of dipolar contacts. For H132A-hHO-hemin-CN, the decreased dynamic stability led to labile proton exchange rates that necessitated collecting NMR data at pH 7.1, at which value a sample stable to precipitation over the 24 h needed for data collection could be maintained only at ≤0.7 mM. The low concentration makes it impractical to collect data of the same quality as for WT, but still allows significant conclusions.

NMR Spectroscopy. ^{1}H NMR data were collected over the temperature range 20−30 °C on a G.E. Omega 500 operating at 500 MHz and processed using the MSI software, Felix 950. Reference spectra were collected using a standard 1-pulse experiment with saturation of the water resonance. Spectra were referenced to the residual water peak through 2,2-dimethyl-2-silapentane-5-sulfonate (DSS). WEFT spectra[34] were collected using recycle times ranging from 40 to 200 ms. T_1 data were collected with a standard inversion−recovery sequence and were processed using a linear fit of the initial data points in a plot of intensity vs relaxation delay. The distance to the iron for a proton of interest *i*, R_{Hi}, is obtained from the relation

$$R_{Hi} = [T_1(\text{heme } CH_3) R^6_{Fe-CH_3}/T_1(H_i)]^{1/6} \quad (1)$$

where $R_{Fe-CH_3} \approx 6.1$ Å. Labile protons which exhibit saturation transfer were detected using a 1:1 jump-and-return pulse sequence.[35] Steady-state NOE spectra were collected by selective irradiation of the peak of interest to >90% saturation as described previously.[36] NOESY spectra[37,38] were collected using a 40-ms mixing time and a bandwidth of 21.5 kHz to cover the complete spectral window with a recycle time of 400 ms, and of 12.0 kHz to cover the diamagnetic window under better resolution, in each case using 2048 t2 points for 512 t1 blocks. The numbers of scans per blocks are 162 and 318 for the 12.0- and 21.5-kHz windows, respectively, with the total data acquisition time of ~20 h. Clean TOCSY spectra[39] were collected over the same two bandwidths using a MLEV-17[40] mixing time of 13 ms. Data were processed using 30° sine-squared bell apodization in both dimensions, and zero-filled to 2048 t1 × 2048 t2 data points prior to Fourier transformation.

Results

Substrate-Free hHO. The ^{1}H NMR spectrum of hHO in ^2H_2O is typical of a highly folded globular protein (not shown). Limited 2D ^{1}H NMR studies were carried out with an emphasis on characterizing a cluster of aromatic residues to be subsequently shown to serve as the heme substrate binding site. This characterization, moreover, was found effective only in ^2H_2O solution, where reasonably well-resolved NOESY cross-peaks are dominated by intra- and interaromatic ring contacts as well as contacts between these ring protons and upfield ring-current-shifted aliphatic residues. TOCSY (13-ms mixing time) spectra (not shown) reveal relatively narrow cross-peaks for ~18 relatively mobile aromatic rings, of which 12 (labeled by italic lower case letters *a*−*i*) are of interest herein. A nine-ring (*a*−*i*) cluster will be shown to constitute the substrate binding site, whereas the other three (*j*−*l*) serve as convenient markers for conservation of structure upon substrate binding. The rings are labeled Trp, Phe, and Arom when three, two, and one, respectively, TOCSY cross-peaks are observed (not shown); Arom can be a Tyr or a Phe with nearly degenerate shifts for two of the ring protons. The TOCSY cross-peaks for three isopropyl fragments are detected in the spectral window near 0 ppm (not shown) and are labeled residues *m*−*o*. NOESY spectra (not shown; see Supporting Information) reveal that the nine aromatic rings (*a*−*i*) and the three Leu/Val fragments (labeled *m*−*o*) exhibit interresidue dipolar contacts indicative of a cluster as described schematically in Figure 1. In addition, there are numerous common dipolar contacts to other protons whose spin system could not be ascertained because of spectral crowding. In parentheses by each residue in Figure 1 are the observed numbers of ring proton cross-peaks to the aliphatic region which likely correlate with the degree that the residue is buried in the protein interior. The three remaining rings (Arom *j*, Phe *k*, and Trp *l*) are relatively isolated from other aromatic rings and have environments that are minimally perturbed upon substrate binding (see below). The backbone of the rings could be elucidated only for Phe *a* and Arom *j*, whose $C_\alpha H$ resonate in the relatively uncrowded window near 5 ppm. The chemical shifts for the aromatic rings *a*−*l* and the three aliphatic fragments *m*−*o* are listed in Supporting Information.

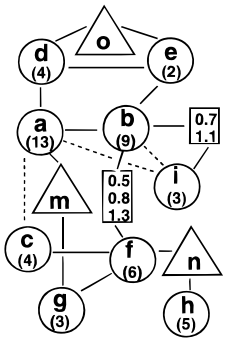

Figure 1. Schematic representation of the dipolar contacts observed among a cluster of aromatic residue side chains (circles labeled a−i) and their aliphatic (triangles labeled m−o) contacts in diamagnetic, substrate-free hHO. Directly detected dipolar contacts between aromatic rings (circles) are shown by solid lines connecting the appropriate residues; dipolar contacts implied by multiple common aliphatic contacts, but that cannot be resolved due to degeneracy, are shown by dashed lines. NOESY cross-peaks to common aliphatic protons from unspecified residues are shown in rectangles, with the chemical shifts, in ppm, given. In parentheses within each ring are the number of observed dipolar contacts to aliphatic protons.

High-Spin, Substrate-Bound hHO. The binding of hemin results in a series of poorly resolved, strongly low-field contact-shifted signals arising primarily from the heme, as shown previously for the rHO-hemin complex.[24] The TOCSY and NOESY maps (not shown) in the aromatic window exhibit a very significantly reduced number of relatively narrow intra-ring cross-peaks relative to substrate-free hHO, of which only three closely resembled the aromatic residues observed in substrate-free hHO, namely the "isolated" rings of Arom *j*, Phe *k*, and Trp *l* (shifts given in Supporting Information).

Low-Spin, Substrate-Bound, Cyanide-Inhibited hHO. (i) Sample Heterogeneity. The normal "diamagnetic" portion of the 500-MHz ^{1}H NMR spectrum of hHO-hemin-CN closely resembles that of substrate-free hHO (not shown), arguing against any global structural transition associated with substrate binding. The resolved low- and high-field portions of the 500-MHz ^{1}H NMR spectra of hHO-PH-CN in ^2H_2O immediately after addition of hemin in the presence of excess cyanide are shown in Figure 2A, and that after 3 days under the same condition is shown in Figure 2B; the spectrum shows no further

(34) Gupta, R. K. *J. Magn. Reson.* **1976**, *24*, 461−465.
(35) Plateau, P.; Gueron, M. *J. Am. Chem. Soc.* **1982**, *104*, 7310−7311.
(36) Thanabal, V.; de Ropp, J. S.; La Mar, G. N. *J. Am. Chem. Soc.* **1987**, *109*, 265−272.
(37) Jeener, J.; Meier, B. H.; Bachmann, P.; Ernst, R. R. *J. Chem. Phys.* **1979**, *71*, 4546−4553.
(38) States, D. J.; Haberkorn, R. A.; Reuben, D. J. *J. Magn. Reson.* **1982**, *48*, 286−292.
(39) Griesinger, C.; Otting, G.; Wüthrich, K.; Ernst, R. R. *J. Am. Chem. Soc.* **1988**, *110*, 7870−7872.
(40) Bax, A.; Davis, D. G. *J. Magn. Reson.* **1985**, *65*, 355−360.

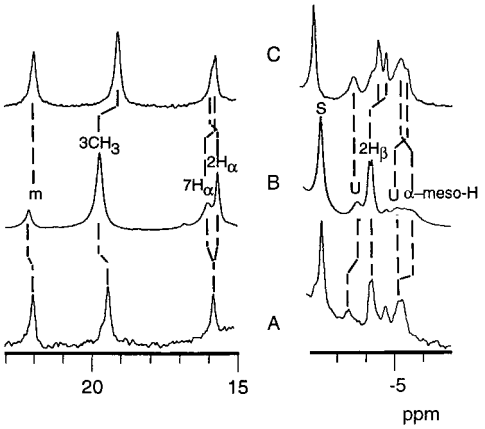

Figure 2. Resolved portions of the 500-MHz ^{1}H NMR spectra of hHO-hemin-CN (A) immediately after binding hemin in the presence of CN^- and (B) after 3 days when the sample had come to equilibrium with a residual 3:1 ratio of major to minor isomers and (C) of equilibrated rHO-hemin-CN showing the 55:45 heme orientational disorder. All spectra are in ^2H_2O, pH 8, at 25 °C. Assigned peaks for the heme, residue *U*, and Ala *S* are labeled.

changes with time. Figure 2A exhibits two sets of peaks whose relative intensities change with time, reaching an equilibrium ratio of ~3:1 (Figure 2B). The same initial 1:1 heterogeneity was observed[24] in rHO−PH−CN, but with a resulting equilibrium heterogeneity of ~55:45 (Figure 2C). Thus, hHO initially binds the substrate in either orientation about the heme α,γ-meso axis, but there is a much stronger preference for one equilibrium orientation in hHO than in rHO, making the former protein a significantly superior candidate for ^{1}H NMR investigation. The number and relative intensities of the major isomer resolved resonances in the cyanide-inhibited, substrate-bound rHO and hHO complexes are very similar. Subsequent consideration focuses on the major isomer of hHO-hemin-CN, and the minor isomer is addressed only as it interferes with definitive assignment of the major isomer. Because of severely reduced solubility and extreme pH effects on chemical shifts at acidic to neutral pH, the optimal pH for reproducible 2D ^{1}H NMR data on hHO-hemin-CN was found to be pH ~8.

(ii) Assignment Protocols. Because of the strong influence on aromatic side-chain cross-peaks of adding hemin to hHO, we first carry out a characterization of the aromatic side chains similar to that reported above for apo-HO. This is followed by the unambiguous assignment of the heme and axial His resonances. Last, we characterize by scalar connectivity (side-chain type) the residues in dipolar contact with the heme and/or axial His, or those that exhibit significant hyperfine shifts (temperature-dependent shifts) and/or paramagnetic relaxation.[41,42] These latter residues are partitioned into proximal and distal residues, as evidenced by relaxation properties relative to a heme methyl that force the residue to lie on one or the other side, as supported by the presence or absence of dipolar contact to the axial His.

(iii) Aromatic Residues. 2D NMR spectra for the 5−10-ppm spectral window involving nonlabile protons were vastly superior in ^2H_2O compared to ^1H_2O due to the large number of NOESY cross-peaks from labile protons (not shown). Moreover, TOCSY spectra reveal surprisingly few $N_pH-C_\alpha H$ correlations in ^1H_2O at the pH ~8 required for stable sample solubility. This precludes standard sequence-specific assignment

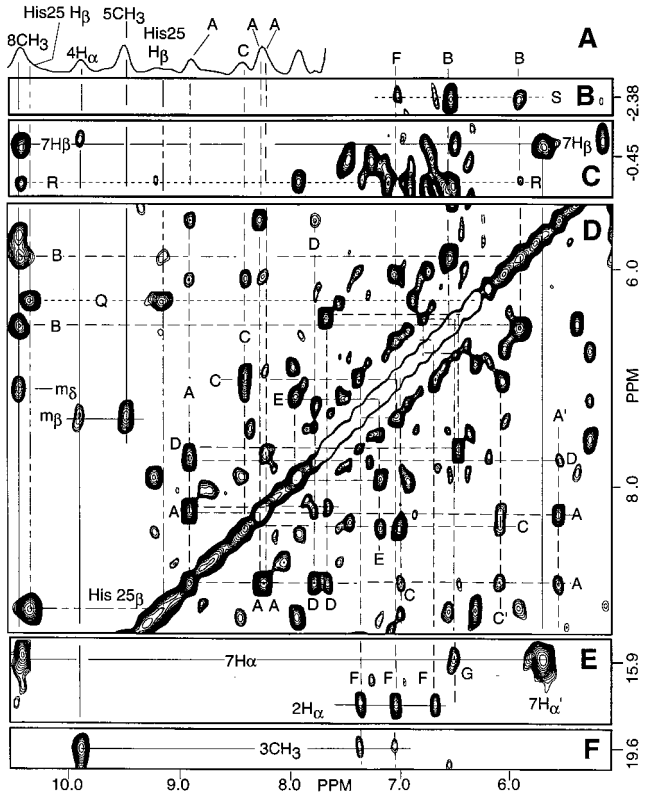

Figure 3. (A) WEFT reference spectrum for hHO-hemin-CN in ^2H_2O at 25 °C, pH 8.0, for the 8−11-ppm window; resolved peaks are labeled as assigned. (B−F) Portions of the NOESY spectrum (40 ms mixing time, repetition time 400 ms) showing key intraresidue (also detected by TOCSY) and interresidue NOESY cross-peaks for relaxed and hyperfine-shifted residues. The various types of protons are identified for the heme (—), axial His25 (—••—), aromatic side chain (- - -), and aliphatic side chains (•••). The heme peaks are labeled by the Fisher notation and residues are labeled by uppercase letters A−Z that represent an arbitrary label for all residues with shifts listed in Table 1.

of residues by their backbone connectivities. Hence, all 2D NMR was initially carried out in ^2H_2O, and ^1H_2O 2D maps were subsequently inspected for the impact of labile protons on the scalar and dipolar connectivities of interest.

A combination of slow (not shown; see Supporting Information) and rapid repetition rate TOCSY (not shown) and NOESY (Figure 3D) data reveal intraresidue cross-peaks for ~18−20 aromatic rings, of which nine, labeled *A-I*, are of interest here. Three other rings exhibit essentially the same shifts and dipolar contacts as Arom *j*, Phe *k*, and Trp *l* of hHO and hHO-hemin and are of no further interest except to confirm conserved structures remote from the substrate; the shifts are listed in Supporting Information. In addition, four upfield TOCSY-detected aliphatic residue fragments, labeled *M*−*P*, are observed to interact with a number of the nine aromatic rings *A*−*I* (not shown). Cross-peak intensities as a function of repetition time reveal rings whose paramagnetic relaxivity is weak (T_1 > 150 ms; Phes *F*, *I*), moderate (100 < T_1 < 150 ms; Phes *A*, *D*, Aroms *C*, *E*, *G*, and *H*), and strong (T_1 < 100 ms; Arom *B*). The interresidue NOESY cross-peaks (Figure 3D; Supporting Information) show that aromatic rings *A*−*I* participate in three "clusters", with cluster **4A** containing four rings (Phes *A*, *D*, Aroms *C*, *E*; NOESY data shown in Figure 3D), cluster **4B** containing two rings (Phes *F*, *I*), and cluster **4C** involving three rings (Aroms *B*, *G*, *H*), as shown schematically in Figure 4. Clusters **4A** and **4B** are connected via dipolar contact between aliphatic residues *M* and *N* (data not shown). The backbone

(41) Qin, J.; La Mar, G. N. *J. Biomol. NMR* **1992**, *2*, 597−618.
(42) Chen, Z.; de Ropp, J. S.; Hernández, G.; La Mar, G. N. *J. Am. Chem. Soc.* **1994**, *116*, 8772−8783.

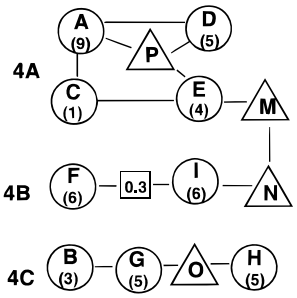

Figure 4. Schematic representation of the dipolar contacts observed among a cluster of aromatic residue rings (circles labeled A−L) and their aliphatic residue (triangles labeled M−P) contacts in hHO−PH−CN. The solid lines indicate interresidue NOESY cross-peaks. NOESY cross-peaks to common aliphatic protons from unspecified residues are shown in rectangles, with the chemical shifts, in ppm, given in the rectangle. In parentheses below the aromatic ring labels are given the number of observed dipolar contacts to aliphatic protons.

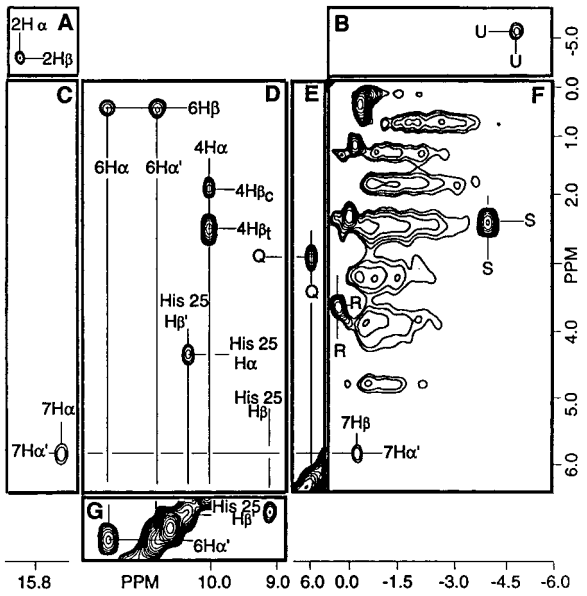

Figure 5. Portions of the 500-MHz TOCSY spectrum (13 ms mixing time, repetition time 400 ms) of hHO-hemin-CN in ^2H_2O at 25 °C, pH 9, illustrating scalar connectivities among strongly relaxed protons for the heme substituents, axial His25 $C_\beta H_2-C_\alpha H$ fragment, Ala *S*, Ala *R*, residue *Q*, and residue *U*. Heme protons are identified by the Fisher notation, and assigned residue protons are labeled by upper caseletters A−Z that represent an arbitrary label for the residues with chemical shifts listed in Table 1.

could be assigned only for Phes *A* and *C* because the C_αHs resonate in the relatively uncrowded 5−6-ppm window (protons A′ and C′ in Figure 3D).

(iv) Heme and Axial His Assignment. Several key heme signals are conveniently detected in the 8−11-ppm portion of a WEFT spectrum shown in Figure 3A. Combination of rapid repetition rate TOCSY (Figure 5) and NOESY (Figure 6) spectra in ^2H_2O leads to the complete assignment of the heme by the standard dipolar connectivity about the heme periphery (Figure 6). These connections involve the four TOCSY-detected vinyl and propionate side chains (Figure 5A,C,D,F,G), the four methyls with no TOCSY connectivity, and the four strongly relaxed ($T_1 \approx 35$ ms) meso-H with no TOCSY connectivity but strongly low-field intercepts in Curie plots.[41,42] The chemical shifts, nonselective T_1s, and slopes in a Curie plot are listed in Table 2, where they are compared with more limited data previously reported[24] for rHO-PH-CN.

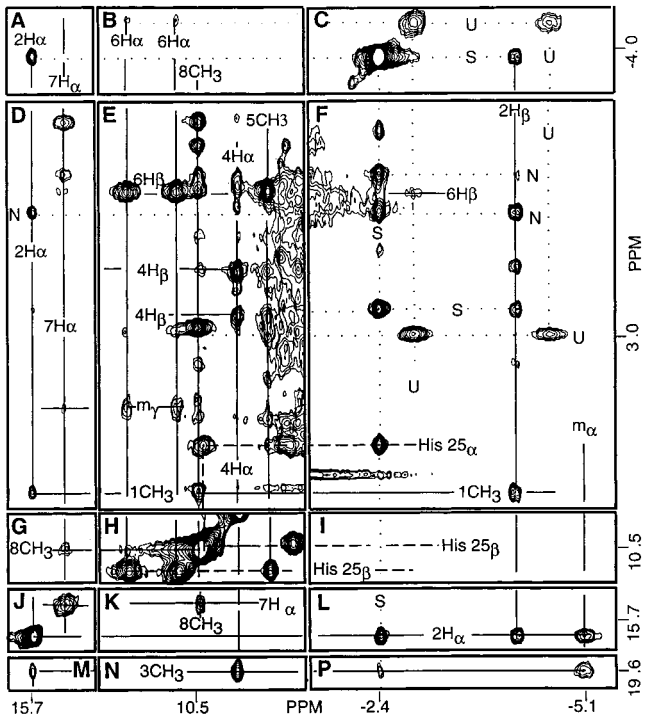

Figure 6. Portions of the NOESY map (40 ms mixing time, repetition rate 400 ms) of hHO-hemin-CN in ^2H_2O at 25 °C, pH 9, illustrating dipolar contact among strongly relaxed resonances of the heme, axial His25, Ala *S*, and residue *U*. Heme protons are identified by the Fisher notation, and unassigned residue protons are labeled by upper caseletters A−Z that represent an arbitrary label for the residues with chemical shifts listed in Table 1. Heme protons are labeled by solid lines, His25 proton by dashed lines, and aliphatic residue protons by dotted lines.

A common characteristic of all low-spin ferrihemoproteins is that the C_βHs of the axial His exhibit substantial contact shifts, with at least one of the two C_βHs resolved to the low field of 9 ppm.[30,31,41−43] TOCSY (Figure 5D,G) and NOESY spectra (Figures 3D and 6H,E) reveal that the remaining low-field and strongly relaxed ($T_1 \approx 70$ ms) single-proton peak at 9.3 ppm (Figure 3A) exhibits the scalar and dipolar connectivity to two protons that are diagnostic of the $C_\beta H_2-C_\alpha H$ of His25. TOCSY spectra in ^1H_2O failed to resolve an additional cross-peak to the $C_\alpha H$, and neither $C_\beta H$ exhibited a NOESY cross-peak to the His ring $N_\delta H$, as generally observed in globins.[41,43] It is concluded that the axial His $N_\delta H$ and peptide NH most likely exchange rapidly with solvent at this pH. The very strongly relaxed (expected $T_1 \approx 3$ ms) axial His ring CHs are likely under the diamagnetic envelope, with one apparent under the high-field shoulder in a WEFT spectrum[24] (not shown). The chemical shifts and T_1s are listed in Table 2. This accounts for all low-field resolved nonlabile proton peaks and leaves unassigned three upfield-resolved peaks labeled S, U, U in Figure 2B.

(v) Other Proximal Residues. Aromatic cluster **4C** in Figure 4 is unambiguously located on the proximal side (Arom *B* ring, $T_1 \approx 80$ ms; $R_{Fe} \approx 5$ Å) by its NOE to His25 C_βHs (Figure 3D), and the Arom *B* to 8-CH_3 (strong; Figure 3D) and to 1-CH_3 (weak; not shown), Arom *G* to 7H_α (Figure 3E) NOESY cross-peaks place cluster **4C** over pyrrole IV and the pyrrole I/IV junction, as shown schematically in Figure 7. The single-ring TOCSY peak and a NOESY cross-peak from a labile proton to a ring proton indicate that Arom *B* is a Tyr. Arom(Tyr) *B* makes two further key contacts. One is to a TOCSY-detected (Figure

(43) Emerson, S. D.; La Mar, G. N. *Biochemistry* **1990**, *29*, 1556−1566.

Table 1. NMR Spectral Parameters for Nonligated Residues in HHO-PH-CN

label	side chain	chemical shift[a]
A	Phe	8.81(6.4), 8.14(6.3), 8.10(7.5)[b]
B	Tyr	6.45(2.1), 5.81(2.0), *8.16*[c]
C	Arom	8.30(5.9), 6.91(5.7)
D	Phe	7.69(5.9), 7.5(6.4), 6.35(4.7)
E	Arom	6.99(4.0), 7.71(6.5)
F	Phe	7.37, 6.96, 6.62
G	Arom	6.44, 6.78
H	Arom	6.36, 6.93
I	Phe	6.97, 7.08, 7.46
J	aliphatic	2.71(−0.6)
M	aliphatic ($(CH_3)_2CH$)	−0.23, 0.22, 1.27
N	aliphatic (CH_3-CH)	−0.14, 0.43, 1.06
O	aliphatic ($(CH_3)_2CH$)	0.10, 0.22, 0.35, 3.24
P	aliphatic ($(CH_3)_2CH$)	−0.11, 0.09, 2.21
Q	Val 24(?)	6.23(0.8), 3.05(2.5), 2.97(−10), 4.2(4.0), *8.1*
R	Ala	0.02(1.0), 3.61(3.6)
S	Ala	−2.38(8.5) [140 ms],[d] 2.24(5.8)
T	aliphatic	5.20(4.2), 2.7(2.5)
U	Asp(?)	−5.5(10) [35 ms], −3.6(9) [50 ms], 3.1
V	aliphatic	0.91(7.9)
W	Tyr	*16.4* [18 ms], 8.80(5.0), 7.78(6.0)
X	His	*6.84* [80 ms], 7.6, 7.8 ppm
Y	His132	*14.23*, 7.72, 7.51
Z	His	*14.60*, 7.05, 6.8

[a] Shifts in ppm from DSS in ^2H_2O, pH 8.0, at 25 °C, except for labile protons (shown in italics), which are in ^1H_2O. [b] Apparent intercepts, in ppm referenced to DSS, at $T^{-1} = 0$, in a Curie plot for protons with significant dipolar shifts, are given in parentheses after shift. [c] Shifts in italics are for labile protons. [d] Nonselective T_1s, in ms, for resolved or partially resolved resonance are given in square brackets.

5F), moderately relaxed Ala *R* with weak upfield dipolar shifts (Figure 3C), whose NOEs to 8-CH_3 (Figure 3C) and 1-CH_3 (not shown) place it at the proximal pyrrole I/IV junction. The other contact is to a strongly relaxed and upfield dipolar-shifted, resolved methyl ($T_1 \approx 140$ ms, $R_{Fe} \approx 6.2$ Å) (Figure 3B), spin-coupled (Figure 5F) to a strongly upfield dipolar-shifted single proton which is characteristic of another Ala (labeled Ala *S*). The Ala *S* CH_3 NOESY cross-peak to His25 $C_\alpha H$ (Figure 6F), $3CH_3$ (Figure 6P), and $2H_\alpha$ (Figure 6L) clearly places it on the proximal side over the pyrrole I/II junction, as shown schematically in Figure 7.

The only other dipolar contact for His25 is to a strongly low-field-shifted proton (Figure 3D) which is spin-coupled (Figure 5E) to two strongly low-field-shifted protons for a residue labeled Q. The low-field proton is spin-coupled to an obvious NH-$C_\alpha H$, indicating that residue *Q* is a Val. The low-field dipolar shift, together with the presence of a Val conserved in hHO and rHO (for which the same contacts are observed), supports the assignment of residue *Q* as Val24. The absence of NOESY cross-peaks to either the heme, cluster **4C**, or Ala *S* place residue *Q* on the *proximal* side in the vicinity of pyrrole II and the pyrrole II/III junction, as shown in Figure 7. Interestingly, both residue *Q* (Val24) and Arom(Tyr) *B* fail to exhibit NOESY cross-peaks to any residue not in contact with the heme.

The heme 3-CH_3 makes dipolar contacts to two aliphatic protons with significant dipolar shifts. A strong NOESY cross-peak to a proton at 0.9 ppm with very *substantial upfield dipolar shift* (not shown) but with no detectable TOCSY cross-peak is assigned to an aliphatic residue *J*; a weak NOE to Phe *F* indicates a proximal origin. The other proton, with an NOE to the 3-CH_3 at 2.7 ppm, exhibits a sizable *low-field dipolar shift* for an aliphatic residue *V*. The absence of a NOESY cross-peak between the residue *J* and *V* protons, despite contact to 3-CH_3, argues for placing residue *V* on the opposite, or distal, side from residue *J*. Consideration of the pattern of dipolar shifts supports such placement of these two residues (see Discussion). Last, Phe *F* of cluster **4B** exhibits NOESY cross-peaks to both $2H_\alpha$, 3-CH_3 (Figure 3E,F), as well as Ala *S* methyl (Figure 3B), placing it adjacent to the pyrrole I/II junction. Residue *N* in Figure 4, moreover, shows a strong contact to the Ala *S* CH_3 (Figure 6F). The only weak relaxation and minimal dipolar shifts for cluster **4B** rings place it more likely at a peripheral rather than at the proximal position relative to the heme (see below). Thus, numerous residues are in contact with the proximal heme at all but pyrrole III, as shown in Figure 7. Neither the 5-CH_3 nor $4H_\alpha$ exhibits significant intense NOESY cross-peaks that involve non-heme protons. The chemical shifts and T_1 values for proximal residues are included in Table 1.

(vi) Distal Residues. In the absence of any definitive information on distal residues, assignment of residues to the distal side has to be based on the presence of relaxation and dipolar shifts and the *absence* of dipolar contacts to the numerous located proximal residues that contact all but pyrrole III. The only remaining unassigned *resolved* signals are those upfield (Figure 2B), labeled *U* (for residue *U*), which exhibit a TOCSY (Figure 5B) and strong NOESY (Figure 6C) cross-peaks between them despite extreme paramagnetic relaxation, T_1s $\approx$ 35, 55 ms. While neither peak exhibits additional TOCSY cross-peaks, they both exhibit sizable NOESY cross-peaks to a proton at ~3 ppm (Figure 6F), which we assign as the third proton of an AMX spin system (but for which relaxation likely interferes with detection of the vicinal cross-peaks). Residue *U* protons exhibit NOESY cross-peaks (or steady-state NOEs; not shown) to the heme $6H_\alpha$s, $6H_\beta$s (Figures 6B,F) but to no other proton. The relaxivity places (via eq 11) the resolved residue *U* protons ~4.5 and ~5.0 Å from the iron and, in the absence of NOESY cross-peaks to the axial His (or any other proximal residue), necessarily demands that the side chain of residue U is highly isolated and *lies close to the iron over pyrrole III on the distal side of the heme*.

The cluster **4A** rings fail to exhibit NOESY cross-peaks to any of the numerous assigned proximal residues. Hence, the significant dipolar shifts and relaxation argue for a distal side location for the cluster. The cluster **4A** rings do not exhibit NOESY cross-peaks to the heme; however, weak steady-state NOEs to Phe *A* and Phe *E* upon saturating the 3-CH_3 (not shown), a NOESY cross-peak from Phe *A* to distal residue *K*, and a NOESY cross-peak between residue *M* of cluster **4A** and residue *N* of cluster **4B** on the heme periphery place cluster **4A** on the distal side over the site of attack of the heme, as shown schematically in Figure 7.

The 8-CH_3 exhibits a very strong NOESY cross-peak (Figure 6E) to a moderately relaxed proton at 2.68 ppm, with little temperature dependence, which exhibits a TOCSY cross-peak to a peak at 5.2 ppm with a low-field dipolar shift (labeled residue *T*). The inability to detect additional TOCSY cross-peaks does not allow identification of the residue side chain but suggests a low-field-shifted Ala. The absence of NOESY cross-peaks from residue *T* to the proximal Ala *R* or Arom(Tyr) *B* over pyrrole IV necessarily places residue *T* on the distal side. It is clear that the distal side provides fewer dipolar contacts to the heme than the proximal side. The schematic structure of the active site of hHO is shown in Figure 7.

(vii) Labile Protons. Our interest here is restricted to labile protons sufficiently close to the iron ($R_{Fe} < 6$ Å) to potentially modulate reactivity. One such labile proton, labeled *2* in Figure

Table 2. NMR Spectral Parameters for the Heme and Axial His Protons in HHO−PH−CN

position	hHO-hemin-CN δ_{DSS}(obs)[a]	hHO-hemin-CN δ_{int}[b] ($T^{-1}=0$)	hHO-hemin-CN T_1,[c] ms	rHO-hemin-CN, δ_{DSS}(obs)	H132-hHO-hemin-CN, δ_{DSS}(obs)
1-CH_3	4.95	13		*d*	*d*
3-CH_3	19.63	5	95	22.5	19.79
5-CH_3	9.04	16		10.0	9.03
8-CH_3	10.48	10	120	10.6	10.59
2H_α	15.68	9	86	16.0	15.52
2H_βs	−4.22, −4.23	9	115	−4.8, −5.3	−4.00, −4.19
4H_α	10.09	10		*d*	10.05
4H_βs	1.77, 2.52	∼0		*d*	1.95
6H_α	11.75	5	120	11.9	11.63
6$H_{\alpha'}$	10.62	5	120	11.4	10.77
6H_βs	0.40	1		*d*	0.44
7H_α	15.87	0	100	16.0	15.68
7H_α'	5.68	14		*d*	5.66
7H_βs	−0.45	4		*d*	0.68
α-meso-H	−5.10	16	35	−5.8	−4.99
β-meso-H	7.60	8		*d*	7.22
γ-meso-H	3.84	11		*d*	*d*
δ-meso-H	7.13	10		*d*	*d*
His25 C_βH	9.13	0	86	9.45	9.13
His25 C_βH′	10.19	−2		10.52	10.2
His25 C_αH	4.30	0		*d*	*d*
His25 ring CH	−2.5		<5	−3.0	*d*

[a] Shifts in ppm from DSS, in $2H_2O$, 100 mM in phosphate, pH 8.0, at 25 °C. [b] Intercept, in ppm from DSS, at $T^{-1}=0$, in a Curie plot. [c] Nonselective T_1, in ms. [d] Not assigned.

8A,B, exhibits a resolved peak in the extreme low-field window, with $T_1 \approx 20$ ms ($R_{Fe} \approx 4.5$ Å). Relevant portions of the low-field 40-ms NOESY spectrum are illustrated in Figure 8C,D. Labile proton *2* exhibits a single strong NOESY cross-peak to a presumed nonlabile proton at 8.0 ppm (Figure 8D; a weaker cross-peak is seen at 7.78 ppm), and the two are assigned to a residue *W*, for which peak *2* is a side-chain labile proton. The 8.0-ppm peak exhibits a Curie intercept similar to that shown by other aromatic protons (Table 1). Hence, logical alternative origins for proton *2* and its dipolar contact at 8.0 ppm are a His N_δH with a contact to its C_ϵH, or a Tyr OH with contact to its C_ϵHs. While the expected TOCSY/NOESY cross-peak is not seen from the proposed C_ϵH to C_δHs, a weaker, likely secondary NOESY cross-peak for labile proton *2* to 7.78 ppm would be a candidate for the C_δHs peak, whose shift is insufficiently different from that of C_ϵHs to allow resolution from the diagonal and cross-peaks between these two protons. Most importantly, the short $T_1 \approx 20$ ms ($R_{Fe} \approx 4.5$ Å), in the absence of detectable NOEs to the axial His or the other numerous proximal contacts, places residue *W* in the *distal* pocket.

A second labile proton of interest is observed only in partially relaxed spectra in ^1H_2O and pH ∼8 (signal experiences saturation transfer at pH 9, not shown; see Supporting Information). The proton, labeled *5*, with $T_1 \approx 80$ ms ($R_{Fe} \approx 5.3$ Å) exhibits strong cross-peaks in a rapid repetition rate NOESY spectrum to two partially resolved nonlabile protons with essentially temperature-independent chemical shifts in the aromatic window (not shown; see Supporting Information). The NOESY pattern and shifts allow the assignment of proton *5* as the N_ϵH of a His *X*, with the nonlabile dipolar contact due to the C_ϵH and C_δH of the same His *X*. The failure to detect NOESY cross-peaks from any His *X* proton to the numerous proximal residues strongly suggests, but does not prove, that His *X* is a distal residue. The chemical shifts and T_1s for residues with relaxed labile protons are included in Table 1.

(viii) Other H-Bonding Interactions. The low-field labile protons, *1*, *3*, and *4* in Figure 8A,B, have $R_{Fe} > 6$ Å, display extreme low-field shifts indicative of very strong hydrogen bonds, and exhibit saturation transfer[44,45] (base-catalyzed; not shown) with bulk solvent (Figure 8A,B). Protons *3* and *4* clearly arise from a pair of His rings (labeled His *Y* and His *Z*) N_ϵHs with NOESY cross-peaks to the C_ϵHs and C_δHs in the aromatic window (Figure 8D). It is noteworthy that His *Y* and His *Z* rings also exhibit a pseudosymmetric environment in that they exhibit identical patterns of dipolar contacts in the aliphatic window[46] (Figure 8C). Spectral crowding precluded sequence-specific assignments of these His groups. The chemical shifts are listed in Table 1.

H132A-hHO-Hemin-CN. The chemical shifts for the assigned heme axial His (Table 2) and other assigned residues (see Supporting Information), including the 3:1 equilibrium heme orientation disorder, are essentially the same as those for WT, confirming a strongly conserved structure for the active site. Two differences distinguish the ^{1}H NMR spectra of H132A-hHO-PH-CN and WT-hHO-PH-CN: labile proton peak *3* is missing (see Supporting Information), and all labile protons (including *2* for residue *W*) show significantly more saturation transfer in the former than in the latter complex. We conclude that His *Y* (with labile proton *3*) arises from His132.

Discussion

Efficacy of the NMR Approach. NMR experiments designed to characterize strongly relaxed protons[32,41,42] provided the cross-peaks to map both scalar and dipolar connectivities for the heme and axial His. For strongly relaxed, nonligated residues, it was possible to identify the residue type primarily for resolved signals. The aliphatic envelope was too crowded to yield useful data for all but a few protons on the upfield

(44) Sandström, J. *Dynamic NMR Spectroscopy*; Academic Press: New York, 1982; pp 53−58.

(45) Cutnell, J. D.; La Mar, G. N.; Kong, S. B. *J. Am. Chem. Soc.* **1981**, *103*, 3567−3572.

(46) Four additional, inconsequentially relaxed, partially resolved labile protons in the 10−12-ppm window similarly are involved in H-bond interactions which are pairwise pseudosymmetric in shifts and dipolar contacts (not shown). The nature of these pseudosymmetric H-bond interactions is not known, but since at least one of these residues, His132, is completely conserved, it is likely that the interactions are important in stabilizing the structure required for catalysis.

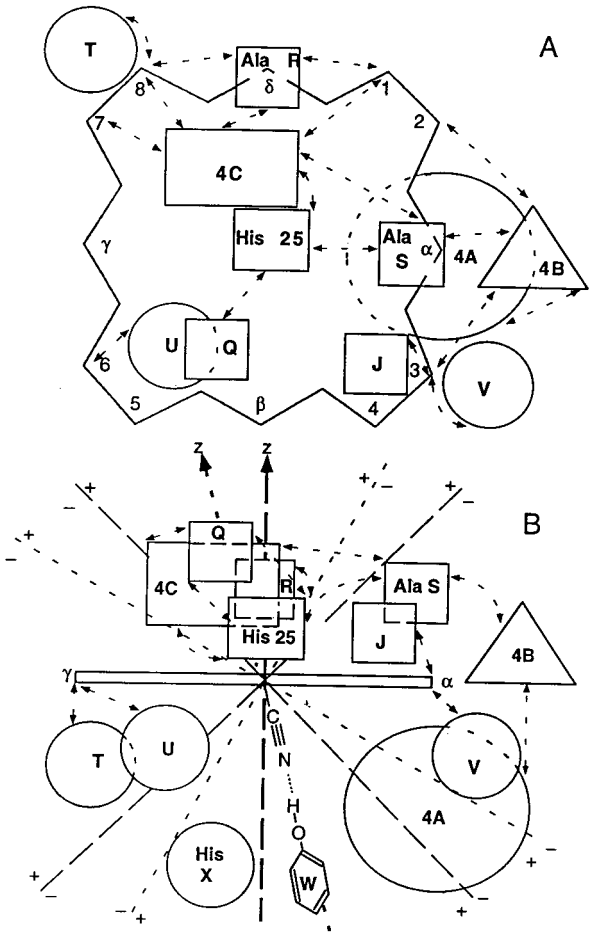

Figure 7. Schematic representation of the substrate binding site in human heme oxygenase as characterized by ^{1}H NMR dipolar contacts to heme, paramagnetic relaxation, and the pattern and direction of dipolar shifts in the hHO-PH-CN complex. (A) Face-on view from the proximal side; (B) edge-on view from the β-meso position. Proximal, peripheral, and distal residues are indicated by rectangles, triangles, and circles, respectively. The major magnetic axis (z' axis) for the case where it is normal to the heme is shown in dark dashed lines, and the nodes of the dipolar shift (magic angle, where $3\cos^2\theta - 1 \approx 0$) are shown by light dashed lines. The major magnetic axis strongly tilted from the normal (z axis) is shown in dark dotted lines, and the nodal surfaces for the dipolar shifts are shown in light dotted lines. The shifts near the respective nodes are designated +/− for downfield/upfield dipolar shifts, respectively.

envelope. The aromatic envelope yielded useful NOESY spectra in ^2H_2O, but even relaxation-edited NOESY in ^1H_2O provided few definitive contacts that could be clearly discerned from artifacts. The severe spectral crowding in the 5−10-ppm window and the broad lines of a 30-kDa protein, together with the rapid exchange with solvent for many peptide NHs at the minimum pH of 8.0 that allowed for a stable NMR sample for 2D NMR, provided the $NHC_\alpha H$ fragments of too few residues to allow sequence-specific assignments. The presence of approximately a 25% population of the minor isomer in hHO, although much better than the 45% population in rHO,[24] also contributed to the spectral crowding. Approaches using much more dilute samples at highly buffered lower pH will be explored. Last, the spin magnetization, as reflected in all dipolar shifts, has a much steeper temperature dependence than in isoelectronic cyanomet globins,[42,43] (i.e., as evidenced by the 8-ppm Curie intercept for the obvious methyl of Ala *S* and the 4-ppm intercept for an obvious ring proton for Phe *A* and Arom

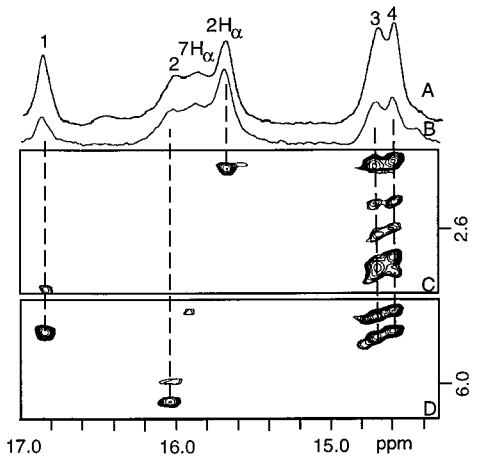

Figure 8. Portions of the extreme low-field 500 MHz ^{1}H NMR spectra of hHO-PH-CN in ^1H_2O at 25 °C, pH 8.0, collected with a 1:1 pulse sequence: (A) without ^1H_2O saturation and (B) with ^1H_2O saturation. The four resolved labile protons are labeled by numbers 1−4, all of which, except peak 2, exhibit significant saturation transfer due to exchange with bulk water. Portions of the NOESY spectrum (40 ms mixing time; 400 ms repetition rate) in the (C) aliphatic spectral window and the (D) aromatic spectral window illustrate the dipolar contacts for the labile protons of interest.

E; Table 1), complicating the interpretation of intercepts in terms of proton functionality.

Nature of the Substrate-Binding Pocket. The NMR data on substrate-free hHO reveal a cluster of at least nine interacting aromatic residues near the protein surface that consist of at least three Phe (Phe *a*, *b*, *f*) and an additional six Tyr or Phe (Figure 1) groups. Phe *a*, *b*, and *f* exhibit large numbers of aliphatic contacts (Figure 1), consistent with their being buried within the protein interior. In contrast, most of the two-spin or likely Tyr rings (i.e., Arom *c*, *d*, *e*, *g*) exhibit minimal aliphatic contacts (Figure 1), suggesting that they are positioned near the protein surface. The bleaching of many of the aromatic signals upon binding high-spin hemin is consistent with paramagnetic relaxation by the high-spin iron. The "reappearance" upon the binding of CN^- of a number of narrow aromatic signals, similar to that seen in substrate-free hHO, argues that the aromatic cluster in hHO is the site of substrate binding. It is a reasonable assumption[47] that the majority of the aromatic residues near the heme in hHO-hemin-CN (Figures 4 and 7) are the same as those that comprise the aromatic cluster in hHO (Figure 1). It appears as if the heme intercalates into the aromatic cluster, with two Phe (*A*, *D*) and two likely Tyr (*C*, *E*) groups forming cluster **4A** on the distal side, three likely Tyr groups positioned on the proximal side in cluster **4C**, and another two Phe groups in cluster **4B**, in contact with the pyrrole ring I and II junction that is the site of oxidation of the heme. The likely key roles of Tyr in these clusters may account for the large number of completely conserved Tyr groups in HO.

While no residues can be sequence-specifically assigned in either complex, the present NMR data allow the following conclusions: (1) the heme pocket of hHO-hemin-CN is much more open than that in globins[48] or heme peroxidases,[49] with

(47) Phe *a* in hHO and Phe *A* in hHO-PH-CN exhibit a very similar dense pattern of NOESY cross-peaks to the aliphatic spectral window, including a cross-peak to an obvious $C_\alpha H$ with a strong, low-field shift even in diamagnetic hHO, and hence can be assumed to represent the same residue. Similar comparison between hHO and hHO-PH-CN for other aromatic rings failed to provide any additional convincing correlations.

(48) Dickerson, R. E.; Geis, I. *Hemoglobin: Structure, Function, Evolution and Pathology*; Benjamin/Cummings: Menlo Park, NJ, 1983.

(49) Poulos, T. L. *Metal Ions Biol. Syst.* **1994**, *30*, 25−76.

the heme exhibiting significantly fewer dipolar contacts to the protein matrix than in other proteins,[41−43] even for the "most buried" portion (the maximum number of non-intraheme NOEs to a heme methyl is the five to the 3-CH_3); (2) the heme is bound with pyrrole I (1-CH_3, 2-vinyl) and parts of pyrroles II (3-methyl) and IV (8-CH_3) buried in the protein interior, while pyrrole III (5-CH_3, 6-propionate) and parts of pyrrole II (4-vinyl) and pyrrole IV (7-propionate) are likely exposed to solvent. The presence of only a few and very weak NOEs for the 4-vinyl and 5-CH_3 is particularly striking. The proximal side is toward the protein *exterior*, as supported by the minimal dipolar contact of the axial His to any residue not in direct contact with the heme, which is in stark contrast to that in globins[41,43,48] and heme peroxidases.[42,49] This inference is also consistent with the fact that both the peptide NH and ring $N_\delta H$ of axial His25 must be in rapid exchange with solvent. A similarly exposed His-binding site is found[50] in cytochromes *c*′. Conversely, two of the residues (Phe *A*, *D*) in the distal aromatic cluster **4A** exhibit a large number of aliphatic contacts, indicative of buried positions; the fewer aliphatic contacts for Arom *C*, *E* support their more solvent exposed position protecting the distal pocket.

Last, while sequence-specific assignments were not attainable in the present study, recent chemical cross-linking of the vinyls to the protein by $CBrCl_3$ identified[51] two peptide fragments, 45−67 and 205−220, linked to vinyls and hence provides candidates for aromatic contacts with the pyrrole I/II junction. These fragments contain two Phe groups, 200 and 213, which are candidates for Phe *F* and/or Phe *A*, Phe *D*, and two Tyr groups, 55 and 213, which are candidates for Arom *E* and/or Arom *C*.

Side-Chain Origin of the Distal Base. The present study finds two residues with labile protons close enough to the iron to modulate ligand reactivity in the distal pocket (His or Tyr), residue *W* (labile proton *2*) and His *X* (labile proton *5*). The His *X* $N_\epsilon H$ is too far away to H-bond to the bound ligand but may play some role in the stereoselectivity, if not the activation of the O_2. The large, low-field dipolar shift and strong relaxation of proton *2*, however, dictate that residue *W* (Tyr or His) is in van der Waals contact with, and likely provides the H-bond to, the bound ligand and must be the distal base with p*K* ∼7.6 in the HO−substrate complex.[23] The relatively minor effect[52] on HO activity of mutating three[9,13,18] of the four conserved His groups and the role of the fourth conserved His25 as axial ligand,[22] together with the present demonstration that labile proton *2* is conserved in H132A-hHO-PH-CN, dictate that the distal base is not a His but a Tyr. Tyr as a distal resdidue that H-bonds to bound ligand has been found in trematode globins.[33,53,54] Mutagenesis studies to identify the distal Tyr are in progress.

Conversely, considering the demonstration that the conserved His132 is one of two pseudosymmetric His groups (*Y* and *Z*) involved in a strong H-bond network[47] relevant to the dynamic stabilization of the substrate pocket (Tyr *W* OH exchanges some factor >10 faster in H132A- than WT-hHO-PH-CN), it is highly likely that the other His *Z* is also a conserved His. Moreover, if the distally placed His *X* is also conserved, this accounts for all conserved His in HO. It is clear that the relationship between His *X*, *Y*, *Z* and the conserved His84, 119, and 132 can be established by mutagenesis and ^{1}H NMR.

Heme Electronic and Magnetic Properties. As suggested[24] by preliminary and partial data on rHO-PH-CN, complete heme assignment of hHO-PH-CN confirms the presence of large π spin density at positions[55] 2, 3, 6, and 7, which reflects an orbital hole with the axial His oriented along the β,δ-meso axis,[56] as shown in Figure 7. The non-Curie behavior for the heme shifts likely reflects thermal population of the excited orbital state as is common to other low-spin ferric hemoproteins.[57] It is noted, however, that since dipolar shift contributions are necessarily the same for α-meso-H as for γ-meso-H (see eq 2 below), the much larger upfield shift for α- than for γ-meso-H dictates the placement of *significant spin density at the* α*-meso position*, and confirms an electronic contribution[19,20] to the activation of the α-meso position for attack. It has been noted[24] in rHO-hemin-CN that the protonation of some residue with p*K* <6 abolishes the unusual heme contact shift pattern and leads to loss of enzyme activity. The noted strong pH sensitivity of residue U and 6-propionate proton chemical shifts to pH indicates a potential role for residue U as the titrating residue that is linked to a propionate and suggests the nature of the residue U spin system as that of an Asp.

The pattern of dipolar shifts, moreover, together with the placement of the residues relative to the heme in Figure 7, allows some qualitative conclusions to be made as to steric influences on bound CN. Dipolar shifts are given by the relation[43,58]

$$\delta_{\mathrm{dip}} = \frac{1}{12\pi N}\left[\Delta\chi_{\mathrm{ax}}\left(\frac{3\cos^2\theta - 1}{R^3}\right) + \frac{3}{2}\Delta\chi_{\mathrm{rh}}\frac{\sin^2\theta\cos 2\Omega}{R^3}\right] \quad (2)$$

where $\Delta\chi_{ax}$ and $\Delta\chi_{rh}$ are the molar anisotropies of the diagonal susceptibility tensor and θ, r, and Ω are the polar coordinates of protons in the magnetic coordinate system. Thus, if the major magnetic (*z*) axis is normal to the heme (as shown by dashed lines in Figure 7), residues *U*, *Q*, and Ala *S* would be close to the nodal plane and experience minimal dipolar shift. However, if the major magnetic axis is *tilted strongly toward the* α*-meso position on the distal side* (shown by dotted lines), residue *U* and Ala *S* would be expected to exhibit large upfield, while residue *Q* would be expected to exhibit large, low-field dipolar shifts, as is observed. The smaller, low-field, rather than high-field, dipolar shift for the ring of cluster **4A** is consistent with such a tilt, as are the opposite direction of the dipolar shifts for residues *V* and *J*. The tilt of the magnetic axes has been correlated in cyanomet Mbs with the Fe−CN tilt induced by steric destabilization of the usual Fe−CN orientation normal to the heme.[43,59] The direction of tilt would favor the O_2 orientation directed toward the α-meso-H position. Steric tilting

(50) Finzel, B. C.; Weber, P. C.; Hardman, K. D.; Salemme, F. R. *J. Mol. Biol*. **1985**, 627−643.

(51) Wilks, A.; Medzihradszky, K. F.; Ortiz de Montellano, P. R. *Biochemistry* **1998**, *37*, 2889−2896.

(52) The relatively minor effect of His mutation on HO activity is to be contrasted to the decrease by a factor 10^6 in activity upon substituting the distal His in horseradish peroxidase (Newmyer, S. L.; Ortiz de Montellano, P. R. *J. Biol. Chem.* **1995**, *270*, 19430−19438).

(53) De Baere, I.; Perutz, M. F.; Kiger, L.; Marden, M.; Poyart, C. *Proc. Natl. Acad. Sci. U.S.A.* **1994**, *92*, 4224−4228. Yang, J.; Kloek, A. P.; Goldberg, D. E.; Mathews, F. S. *Proc. Natl. Acad. Sci. U.S.A.* **1995**, *92*, 4224−4228.

(54) Zhang, W.; Rashid, K. A.; Haque, M.; Siddiqi, A. H.; Vinogradov, S. N.; Moens, L.; La Mar, G. N. *J. Biol. Chem.* **1997**, *275*, 3000−3006.

(55) For a propionate $C_\alpha H$, the contact shift is only about one-half as large as that for a methyl for the same pyrrole carbon π spin density (La Mar, G. N. In *NMR of Paramagnetic Molecules*; La Mar, G. N., Horrocks, W. D., Jr., Holm, R. H., Eds.; Academic Press: New York, 1973; Chapter 2).

(56) Tan, H.; Simonis, U.; Shokhirev, N. V.; Walker, F. A. *J. Am. Chem. Soc*. **1994**, *116*, 5784−5790.

(57) Shulman, R. G.; Glarus, S. H.; Karplus, M. *J. Mol. Biol*. **1971**, *57*, 93−115.

(58) La Mar, G. N.; Chen, Z.; Vyas, K.; McPherson, A. D. *J. Am. Chem. Soc*. **1995**, *117*, 411−419.

of bound ligands has been noted[27] in the FeO_2 unit in rHO-heme-O_2 and is consistent with the recently reported[21] strong destabilization of bound CO over bound O_2 in rHO-heme, as compared to that in globins.

Conclusions

In summary, the NMR results described here place several clusters of aromatic residues in close proximity to the heme, identify whether the residues are on the proximal or distal side, and indicate that the heme is in a more open environment than it is in myoglobin or horseradish peroxidase. Of particular importance is the finding that a nonhistidine aromatic residue, identified as a tyrosine, hydrogen bonds to the cyanide in the cyano complex. The same tyrosine may hydrogen bond to the ferrous dioxygen complex and thus may have a catalytic role.

Acknowledgment. The authors are indebted to Dr. K. Clark for preliminary 2D NMR data on hHO. This research was supported by grants from the National Institutes of Health, GM 26226 (G.N.L.) and DK 30297 (P.R.O.M.).

Supporting Information Available: Five figures (NOESY spectrum for aromatic protons of hHO and hHO-PH-CN in ^2H_2O, reference spectra of H132A-hHO-PH-CN, 1:1 NMR spectra of H132A-hHO-PH-CN in ^1H_2O, and NOESY spectra for His *X* in WT and H132A-hHO-CN in ^1H_2O) and two tables (chemical shifts for aromatic rings and aliphatic contacts in hHO and for H132A-hHO-PH-CN and rHO-PH-CN) (7 pages, print/PDF). See any current masthead page for ordering information and Web access instructions.

JA9815475

(59) Rajarathnam, K.; La Mar, G. N.; Chiu, M. L.; Sligar, S. G. *J. Am. Chem. Soc.* **1992**, *114*, 9048−9058. Rajarathnam, K.; Qin, J.; La Mar, G. N.; Chiu, M. L.; Sligar, S. G. *Biochemistry* **1993**, *32*, 5670−5680. Rajarathnam, K.; Qin, J.; La Mar, G. N.; Chiu, M. L.; Sligar, S. G. *Biochemistry* **1994**, *33*, 5493−5501.